ISSN 1674-1056
http://cpb.iphy.ac.cn
http://iopscience.iop.org/cpb
中国物理 B
Chinese Physics
中国物理
Chinese Physics B

Nonparaxial propagation properties of the chirped Airy Gaussian vortex beams in uniaxial crystals orthogonal to the optical axis

Yizuo Chen(陈奕佐), Guanwen Zhao(赵官文), Feng Ye(叶峰), Chuangjie Xu(许创杰), Dongmei Deng(邓冬梅)
Citation: Chin. Phys. B . 2018, 27(10): 104201. **doi:** 10.1088/1674-1056/27/10/104201

What follows is a list of articles you may be interested in

A new method of calculating the orbital angular momentum spectra of Laguerre-Gaussian beams in channels with atmospheric turbulence

Xiao-zhou Cui(崔小舟), Xiao-li Yin(尹霄丽), Huan Chang(常欢), Zhi-chao Zhang(张志超), Yong-jun Wang(王拥军), Guo-hua Wu(吴国华)
Chin. Phys. B . 2017, 26(11): 114207. **doi:** 10.1088/1674-1056/26/11/114207

Orbital angular momentum density and spiral spectra of Lorentz-Gauss vortex beams passing through a single slit

Zhi-Yue Ji(季志跃), Guo-Quan Zhou(周国泉)
Chin. Phys. B . 2017, 26(9): 094202. **doi:** 10.1088/1674-1056/26/9/094202

Microscale vortex laser with controlled topological charge

Xing-Yuan Wang(王兴远), Hua-Zhou Chen(陈华洲), Ying Li(黎颖), Bo Li(李波), Ren-Min Ma(马仁敏)
Chin. Phys. B . 2016, 25(12): 124211. **doi:** 10.1088/1674-1056/25/12/124211

Turbulence mitigation scheme based on multiple-user detection in an orbital-angular-momentum multiplexed system

Li Zou(邹丽), Le Wang(王乐), Sheng-Mei Zhao(赵生妹), Han-Wu Chen(陈汉武)
Chin. Phys. B . 2016, 25(11): 114215. **doi:** 10.1088/1674-1056/25/11/114215

The Wigner distribution functions of coherent and partially coherent Bessel–Gaussian beams

Zhu Kai-Cheng,Li Shao-Xin,Tang Ying,Yu Yan,Tang Hui-Qin
Chin. Phys. B . 2012, 21(3): 034201. **doi:** 10.1088/1674-1056/21/3/034201

Nonparaxial propagation properties of the chirped Airy Gaussian vortex beams in uniaxial crystals orthogonal to the optical axis*

Yizuo Chen(陈奕佐), Guanwen Zhao(赵官文), Feng Ye(叶峰),
Chuangjie Xu(许创杰), and Dongmei Deng(邓冬梅)†

Guangdong Provincial Key Laboratory of Nanophotonic Functional Materials and Devices, South China Normal University, Guangzhou 510631, *China*

(Received 21 May 2018; revised manuscript received 20 June 2018; published online 10 September 2018)

In this article, we investigate the nonparaxial propagation properties of the chirped Airy Gaussian vortex (CAiGV) beams in uniaxial crystals orthogonal to the optical axis analytically and numerically. We discuss how the linear chirp parameters, the quadratic chirp parameters, and the Gaussian factors influence the nonparaxial propagation dynamics of the CAiGV beams. The intensity, the energy flow, the beam center, and the angular momentum of the CAiGV beams are deeply investigated. It is shown that the Gaussian factors have a great effect on the intensity and the centroid positions of the CAiGV beams. With the Gaussian factors increasing, the intensity of CAiGV beams decreases rapidly. The main lobes of the transverse intensity distribution of the CAiGV beams are similar to triangles.

Keywords: Chirped Airy Gaussian vortex beams, energy flow, angular momentum, nonparaxial propagation

PACS: 42.25.–p, 42.25.Bs **DOI:** 10.1088/1674-1056/27/10/104201

1. Introduction

Airy beams, one kind of unique beams, were introduced by Berry and Balazs after obtaining the solution of the Schrodinger equation in 1979.[1] However, the energy of the Airy beams is infinite in theory, indicating that it could not be realized experimentally. In 2007, Siviloglou firstly obtained Airy beams with finite energy by means of adding a decay factor.[2] Next year, John Broky discovered the self-healing properties of Airy beams.[3] Due to the excellent properties of Airy beams, such as self-acceleration,[2] non-diffracting, and self-healing,[3] many researchers have shown interest in Airy beams.[4] Then Airy beams were considered in the situation of propagating in free space,[5,6] right-handed material to left-handed material,[7] linear medium,[8] uniaxial crystals,[9] and a quadratic-index medium.[10] Nowadays we can see applications of Airy beams with finite energy in the military,[11] atmospheric science,[12] curved plasma channel generation,[13] and so on.

We can obtain Airy Gaussian vortex (AiGV) beams theoretically by means of adding the Gaussian factor and the vortex factor to the Airy beams, which results in the fact that the AiGV beams not only have excellent features of the Airy Gaussian (AiG) beams,[14] but also have the intensity singularities as well as phase singularities,[15] which are exactly the properties of vortex beams produced by employing synthetic holograms,[16] higher order laser mode separation,[17] and so on.

In the context of optical fiber communication, we define a chirp as a phenomenon for the purpose of describing signal frequency, which changes over time. It was Zhang[18] who introduced a chirp carried by the Airy beams in the domain of optical science, disclosing the fact that the chirps including linear chirps and nonlinear chirps play an important part in modulating beams, involving beam compression as well as pulse generation.

Crystals have been applied in the design of polarizers and compensators. It is significant to describe the light propagation in the anisotropic media theoretically.[19] When the waist radius of the beams is comparable with the wavelength in uniaxial crystals and the far-field divergence angle becomes larger, the paraxial theory is not suitable, so we have to consider the nonparaxial effect of the beams. There are some remarkable papers about such situations.[20,21] However, to the best of our knowledge, the nonparaxial propagation of the chirped Airy Gaussian vortex beams through uniaxial crystals orthogonal to the optical axis has not been investigated yet. The results of our research can be applied in the realm of optical trapping.

The present article is organized as follows. At first in Section 2, we gain the analytical solutions of the CAiGV beams by means of the theoretical model of the nonparaxial propagation in uniaxial crystals orthogonal to the optical axis. Then in Section 3, we discuss the nonparaxial evolutions of the beam intensity and the beam center of the CAiGV beams. We are concerned about how the Gaussian factors and chirp parameters act on the energy flow density and the angular momentum of the linear chirped Airy Gaussian vortex (LCAiGV) beams and the quadratic chirped Airy Gaussian vortex (QCAiGV) beams respectively in Section 4. Finally in Section 5, the paper is summarized.

*Project supported by the National Natural Science Foundation of China (Grant Nos. 11775083 and 11374108)
†Corresponding author. E-mail: dmdeng@263.net
© 2018 Chinese Physical Society and IOP Publishing Ltd

2. Analytic solution of the CAiGV beams in uniaxial crystal orthogonal to the optical axis

We set the z axis to be the propagation axis, and the x axis to be the optical axis of the uniaxial crystals in the spatial coordinate system. Relative dielectric tensor ε of the uniaxial crystals is set as[22]

$$\varepsilon = \begin{pmatrix} n_{\mathrm{e}}^2 & 0 & 0 \\ 0 & n_{\mathrm{o}}^2 & 0 \\ 0 & 0 & n_{\mathrm{o}}^2 \end{pmatrix}, \tag{1}$$

where n_{e} and n_{o} are the extraordinary and the ordinary refractive indices, respectively. For simplicity, we set the center of the vortex of the beam at the origin. The electric field distribution of the CAiGV beams in the input plane is

$$\begin{bmatrix} \boldsymbol{E}_x(x_0,y_0,0) \\ \boldsymbol{E}_y(x_0,y_0,0) \end{bmatrix} = \begin{bmatrix} \mathrm{Ai}\left(\frac{x_0}{w_0}\right)\mathrm{Ai}\left(\frac{y_0}{w_0}\right)\exp\left(\frac{ax_0}{w_0}+\frac{ay_0}{w_0}-\frac{\chi_0^2x_0^2}{w_0^2}-\frac{\chi_0^2y_0^2}{w_0^2}+\right. \\ \left.\mathrm{i}\beta_1\frac{x_0}{w_0}+\mathrm{i}\beta_2\frac{y_0}{w_0}+\mathrm{i}\beta_3\frac{x_0^2}{w_0^2}+\mathrm{i}\beta_4\frac{y_0^2}{w_0^2}\right)\left(\frac{x_0}{w_0}+\mathrm{i}\frac{y_0}{w_0}\right) \\ 0 \end{bmatrix}, \tag{2}$$

where w_0 represents the initial beam waist size; a is the truncation factor of the CAiGV beams; and $\mathrm{Ai}(\cdot)$ denotes the first kind of Airy function. β_1 and β_2 are the linear chirp parameters, while β_3 and β_4 are the quadratic chirp parameters.

Based on the theory of the nonparaxial propagation in uniaxial crystals orthogonal to the optical axis, the electric field of a beam is[22]

$$\boldsymbol{E}_x(x,y,z) = \frac{kn_{\mathrm{o}}}{2\pi\mathrm{i}z}\int_{-\infty}^{+\infty}\int_{-\infty}^{+\infty}\boldsymbol{E}_x(x_0,y_0,0)A_{\mathrm{e}}(r,r_0)\,\mathrm{d}x_0\,\mathrm{d}y_0, \tag{3}$$

$$\boldsymbol{E}_y(x,y,z) = \int_{-\infty}^{+\infty}\int_{-\infty}^{+\infty}\{\frac{\mathrm{i}kn_{\mathrm{o}}}{2\pi z^3}(x-x_0)(y-y_0)\boldsymbol{E}_x(x_0,y_0,0)[A_{\mathrm{e}}(r,r_0)-A_{\mathrm{o}}(r,r_0)]+\frac{kn_{\mathrm{o}}}{2\pi\mathrm{i}z}\boldsymbol{E}_y(x_0,y_0,0)A_{\mathrm{o}}(r,r_0)\}\,\mathrm{d}x_0\,\mathrm{d}y_0, \tag{4}$$

$$\boldsymbol{E}_z(x,y,z) = \frac{\mathrm{i}kn_{\mathrm{o}}}{2\pi z^2}\int_{-\infty}^{+\infty}\int_{-\infty}^{+\infty}\{(x-x_0)\,\boldsymbol{E}_x(x_0,y_0,0)A_{\mathrm{e}}(r,r_0)-(y-y_0)\,\boldsymbol{E}_y(x_0,y_0,0)A_{\mathrm{o}}(r,r_0)\}\,\mathrm{d}x_0\,\mathrm{d}y_0, \tag{5}$$

with $A_{\mathrm{e}}(r,r_0)$ and $A_{\mathrm{o}}(r,r_0)$ being given by

$$A_{\mathrm{e}}(r,r_0) = \exp(\mathrm{i}kn_{\mathrm{e}}z)\exp\left\{-\frac{k}{2\mathrm{i}zn_{\mathrm{e}}}\left[n_{\mathrm{o}}^2(x-x_0)^2+n_{\mathrm{e}}^2(y-y_0)^2\right]\right\}, \tag{6}$$

$$A_{\mathrm{o}}(r,r_0) = \exp(\mathrm{i}kn_{\mathrm{o}}z)\exp\left\{-\frac{kn_{\mathrm{o}}}{2\mathrm{i}z}\left[(x-x_0)^2+(y-y_0)^2\right]\right\}. \tag{7}$$

Substituting Eq. (2) into Eqs. (3)–(5), we can gain three components of the nonparaxial propagation of the CAiGV beams in uniaxial crystal orthogonal to the optical axis, which can be written as

$$\boldsymbol{E}_x(x,y,z) = \frac{kn_{\mathrm{o}}}{2\pi\mathrm{i}zw_0}\exp\left(\mathrm{i}kn_{\mathrm{e}}z-\frac{kn_{\mathrm{o}}^2x^2}{2\mathrm{i}zn_{\mathrm{e}}}-\frac{kn_{\mathrm{e}}^2y^2}{2\mathrm{i}z}\right)(M_1L_2+\mathrm{i}L_1M_2), \tag{8}$$

$$\begin{aligned}\boldsymbol{E}_y(x,y,z) = {} & \frac{\mathrm{i}kn_{\mathrm{o}}}{2\pi z^3w_0}\exp\left(\mathrm{i}kn_{\mathrm{e}}z-\frac{kn_{\mathrm{o}}^2x^2}{2\mathrm{i}zn_{\mathrm{e}}}-\frac{kn_{\mathrm{e}}y^2}{2\mathrm{i}z}\right)[xyM_1L_2+xy\mathrm{i}L_1M_2-xM_1M_2-x\mathrm{i}L_1N_2 \\ & -yN_1L_2-y\mathrm{i}M_1M_2+N_1M_2+\mathrm{i}M_1N_2]-\frac{\mathrm{i}kn_{\mathrm{o}}}{2\pi z^3w_0}\exp\left(\mathrm{i}kn_{\mathrm{o}}z-\frac{kn_{\mathrm{o}}x^2}{2\mathrm{i}z}-\frac{kn_{\mathrm{o}}y^2}{2\mathrm{i}z}\right) \\ & \times[xyM_3L_4+xy\mathrm{i}L_3M_4-xM_3M_4-x\mathrm{i}L_3N_4-yN_3L_4-y\mathrm{i}M_3M_4+N_3M_4+\mathrm{i}M_3N_4],\end{aligned} \tag{9}$$

$$\boldsymbol{E}_z(x,y,z) = \frac{\mathrm{i}kn_{\mathrm{o}}}{2\pi z^2w_0}\exp(\mathrm{i}kn_{\mathrm{e}}z-\frac{kn_{\mathrm{o}}^2x^2}{2\mathrm{i}zn_{\mathrm{e}}}-\frac{kn_{\mathrm{e}}^2y^2}{2\mathrm{i}z})(xM_1L_2+x\mathrm{i}L_1M_2-N_1L_2-\mathrm{i}M_1M_2), \tag{10}$$

where L_n, M_n, N_n, and $(n=1,2,3,4)$ are

$$L_n = D_n\exp(P_n)\mathrm{Ai}(Q_n), \tag{11}$$

$$M_n = D_n\exp(P_n)[W_n\mathrm{Ai}(Q_n)+G_n\mathrm{Ai}'(Q_n)], \tag{12}$$

$$N_n = D_n\exp(P_n)[H_n\mathrm{Ai}(Q_n)+R_n\mathrm{Ai}(Q_n)+F_n\mathrm{Ai}'(Q_n)], \tag{13}$$

where D_n, P_n, Q_n, W_n, H_n, R_n, F_n and $(n=1,2,3,4)$ are given by the following expressions

$$D_n = \sqrt{-\frac{\pi}{b_n}},$$

$$P_n = -\frac{c_n^2}{4b_n}+\frac{c_n}{8a_n^3b_n^2}-\frac{1}{96a_n^6b_n^3},$$

$$Q_n = \frac{1}{16a_n^4 b_n^2} - \frac{c_n}{2a_n b_n}, \quad W_n = -\frac{c_n}{2b_n} + \frac{1}{8a_n^3 b_n^2},$$
$$H_n = -\frac{1}{2b_n}, \quad R_n = \frac{c_n^2}{4b_n^2} - \frac{c_n}{4a_n^3 b_n^3} + \frac{1}{32a_n^6 b_n^4},$$
$$F_n = -\frac{1}{8a_n^4 b_n^3} + \frac{c_n}{2a_n b_n^2},$$

with

$$a_n = w_0, \quad b_1 = -\frac{\chi_0^2}{w_0^2} + \frac{\mathrm{i}\beta_3}{w_0^2} - \frac{kn_\mathrm{o}^2}{2\mathrm{i}zn_\mathrm{e}},$$
$$b_2 = -\frac{\chi_0^2}{w_0^2} + \frac{\mathrm{i}\beta_4}{w_0^2} - \frac{kn_\mathrm{e}}{2\mathrm{i}z}, \quad b_3 = -\frac{\chi_0^2}{w_0^2} + \frac{\mathrm{i}\beta_3}{w_0^2} - \frac{kn_\mathrm{o}}{2\mathrm{i}z},$$
$$b_4 = -\frac{\chi_0^2}{w_0^2} + \frac{\mathrm{i}\beta_4}{w_0^2} - \frac{kn_\mathrm{o}}{2\mathrm{i}z}, \quad c_1 = \frac{a}{w_0} + \frac{\mathrm{i}\beta_1}{w_0} + \frac{kxn_\mathrm{o}^2}{\mathrm{i}zn_\mathrm{e}},$$
$$c_2 = \frac{a}{w_0} + \frac{\mathrm{i}\beta_2}{w_0} + \frac{kyn_\mathrm{e}}{\mathrm{i}z}, \quad c_3 = \frac{a}{w_0} + \frac{\mathrm{i}\beta_1}{w_0} + \frac{kxn_\mathrm{o}}{\mathrm{i}z},$$
$$c_4 = \frac{a}{w_0} + \frac{\mathrm{i}\beta_2}{w_0} + \frac{kyn_\mathrm{o}}{\mathrm{i}z}$$

and $\mathrm{Ai}'(\cdot)$ represents the first-order derivative of the Airy function.

We investigate the nonparaxial propagation properties of the CAiGV beams in uniaxial crystals orthogonal to the optical axis because of the analytical results from Eqs. (8)–(10). We set that $a = 0.2$, $n_\mathrm{o} = 2.616$, $\lambda = 633$ nm, $w_0 = 0.1$ mm, so the Rayleigh distance can be written as $Z_\mathrm{R} = kw_0^2/2 = 4.963$ cm.

3. The transverse intensity distribution and the propagation path

From Figs. 1(a1)–1(c1), the shape of the main lobe of the LCAiGV beams seems like an ellipse, and the intensity of the LCAiGV beams mainly distributes in the main lobe. The number of the side lobes is decreasing, and the shape of the main lobe is not changed as χ_0 increases. However, comparing Figs. 1(a1)–1(c1) with Fig. 1(d1), we can draw a conclusion that the intensity of the whole beam, including the main lobe and the side lobes, decreases with the increase of χ_0. However, the effect on the main lobe is much smaller than

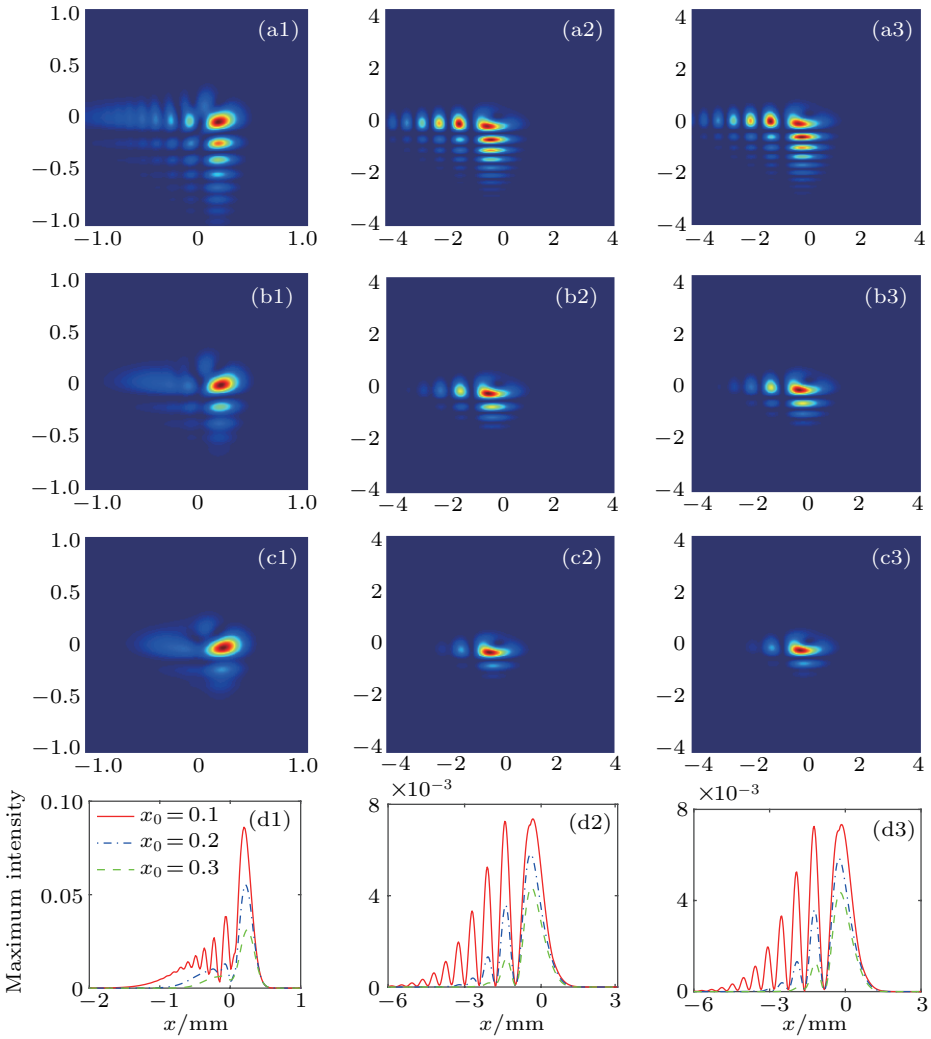


Fig. 1. (color online) Intensity distribution of LCAiGV, QCAiGV, and CAiGV beams with different χ_0 in uniaxial crystals orthogonal to the optical axis on the observation plane $z = 6Z_\mathrm{R}$: (a1)–(a3) $\chi_0 = 0.1$, (b1)–(b3) $\chi_0 = 0.2$, (c1)–(c3) $\chi_0 = 0.3$, (a1)–(c1) the LCAiGV beams with $\beta_1 = \beta_2 = 1$ and $\beta_3 = \beta_4 = 0$, (a2)–(c2) the QCAiGV beams with $\beta_1 = \beta_2 = 0$ and $\beta_3 = \beta_4 = 1$, (a3)–(c3) the CAiGV beams with $\beta_1 = \beta_2 = \beta_3 = \beta_4 = 1$; the maximum evolution of the intensity as a function of x for the LCAiGV beams in panel (d1), the QCAiGV in panel (d2), and the CAiGV beams in panel (d3).

that of the side lobes, so we can only see the main lobe of the beams as χ_0 increases. Then we show the transverse intensity distribution of the QCAiGV beams in Figs. 1(a2)–1(c2), which shows that the shape of the main lobe of the QCAiGV beams seems like a triangle. From Fig. 1(d2), it is shown that the main lobe and the first side lobe have the same maximum intensity, and the larger χ_0 is, the smaller the intensity of the main lobe and the side lobes is. In addition, the distribution of the QCAiGV beams is much more dispersed than that of the LCAiGV beams, and the maximum intensity of the QCAiGV beams is much smaller than that of the LCAiGV beams, comparing Figs. 1(a1)–1(d1) with Figs. 1(a2)–1(d2). So we can draw a conclusion that the quadratic chirp parameters can weaken non-diffracting properties. One can come to a conclusion that the shape and the intensity distribution of the CAiGV beams are mainly influenced by the quadratic chirps from Fig. 1.

The peak intensity distributions of the LCAiGV beams, the QCAiGV beams, and the CAiGV beams with different values of n_e/n_o at different propagation distances are shown in Fig. 2. The peak intensity can be defined as the maximum values of the intensity of each transverse intensity pattern. As for the case of the LCAiGV beams, the larger the values of n_e/n_o are, the smaller the peak intensity of the LCAiGV beams is, when the propagation distance is less than $z = 5Z_R$ and $n_e/n_o \geq 1$. However, the peak intensity of the LCAiGV beams firstly increases, and then decreases with the increase of the propagation distance when $0 < n_e/n_o < 1$. The peak intensity of the LCAiGV beams locates at the position $z = 2Z_R$ when $\chi_0 = 0.2$, while the peak intensity of the LCAiGV beams locates at $z = 1.3Z_R$ when $\chi_0 = 0.3$. As a result the smaller χ_0 is, the further the position corresponding to the peak intensity of the LCAiGV beams is.

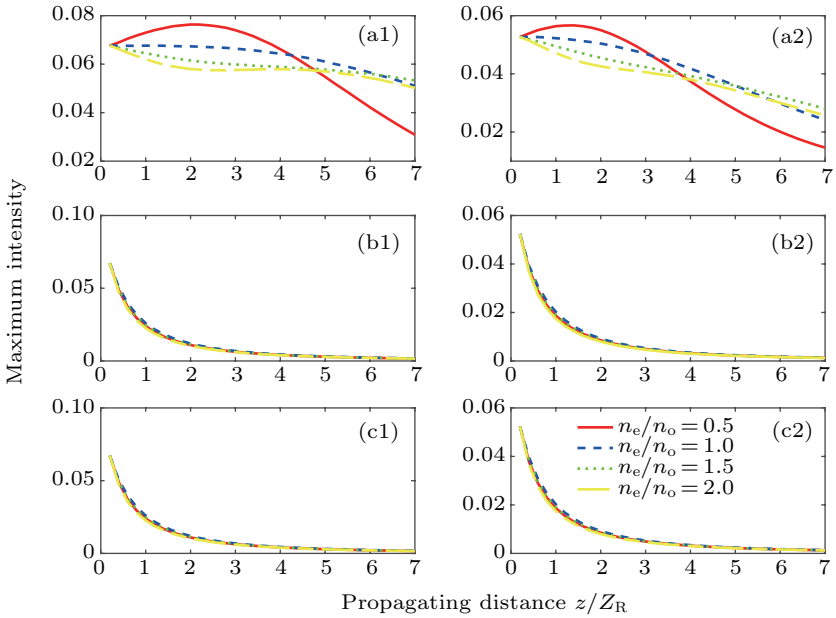


Fig. 2. (color online) Maximum intensity distribution of: (a1)–(a2) the LCAiGV beams, (b1)–(b2) the QCAiGV beams, (c1)–(c2) the CAiGV beams in uniaxial crystals orthogonal to the optical axis with different values of n_e/n_o: (a1)–(c1) $\chi_0 = 0.2$, and (a2)–(c2) $\chi_0 = 0.3$.

As shown in Figs. 2(b1)–2(b2), images of the peak intensity distribution with the different values of n_e/n_o seem like hyperbolas, and all of them are overlapped, which shows that the peak intensity distribution of the QCAiGV beams is irrelevant to n_e/n_o. Similar to the QCAiGV beams, images of the peak intensity distribution of the CAiGV beams also seem like hyperbolas, from which we can draw a conclusion that the quadratic chirp parameters have a decisive influence on the peak intensity distribution of the CAiGV beams. The bigger χ_0 is, the smaller the value of the peak intensity of the CAiGV beams, the LCAiGV beams as well as the QCAiGV beams is.

Based on the numerical calculation, we gain the centroid of the CAiGV beams with different values of χ_0 in Fig. 3. It is shown that the trajectories of the beam center are straight lines no matter when χ_0 is bigger, when the propagation distance is not large. However, on the whole, the centroid of the CAiGV beams complies with the self-bending properties of the Airy beams. In the end, the trajectories of the beam center are parallel to the z axis when the propagation distance is large enough.

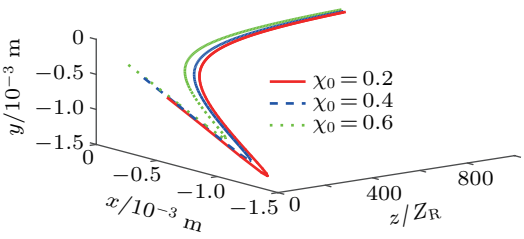


Fig. 3. (color online) The beam center of the CAiGV beams as a function of the propagation distance in uniaxial crystals orthogonal to the optical axis.

4. The energy flow and the angular momentum

In this part we investigate the energy flow and the angular momentum of the LCAiGV beams, and the QCAiGV beams of the nonparaxial propagation in uniaxial crystals orthogonal to the optical axis, respectively. The time averaged Poynting vectors as well as the time averaged angular momentum can be written as[23]

$$\langle \boldsymbol{S} \rangle = \frac{c}{4\pi} \langle \boldsymbol{E} \times \boldsymbol{B} \rangle , \tag{14}$$

$$\langle \boldsymbol{J} \rangle = \boldsymbol{r} \times \langle \boldsymbol{E} \times \boldsymbol{B} \rangle . \tag{15}$$

The transverse energy flow distribution of the LCAiGV beams of the nonparaxial propagation in uniaxial crystals orthogonal to the optical axis is shown in Fig. 4. It is obvious that the energy flux density mainly distributes in the main lobe, while the direction of the arrows is approximately 30° in the positive direction of the x axis. There is an interesting conclusion about χ_0, which indicates that the whole range of the energy density is becoming smaller with the increase of χ_0. We can see that the larger the linear chirp parameters are, the further away the center of the main lobe of the LCAiGV beams from the center of the observation plane is.

Figure 5 shows the energy flow of the QCAiGV beams. The arrows of the energy flow in the area of the side lobes of the x direction approximately point to the positive x axis, while arrows of the energy flow in the area of the side lobes of the y direction are approximately parallel to the y axis, no matter how χ_0 and the quadratic chirp parameters change. The transverse energy flow distribution is becoming more dispersed with the increase of the quadratic chirp parameters.

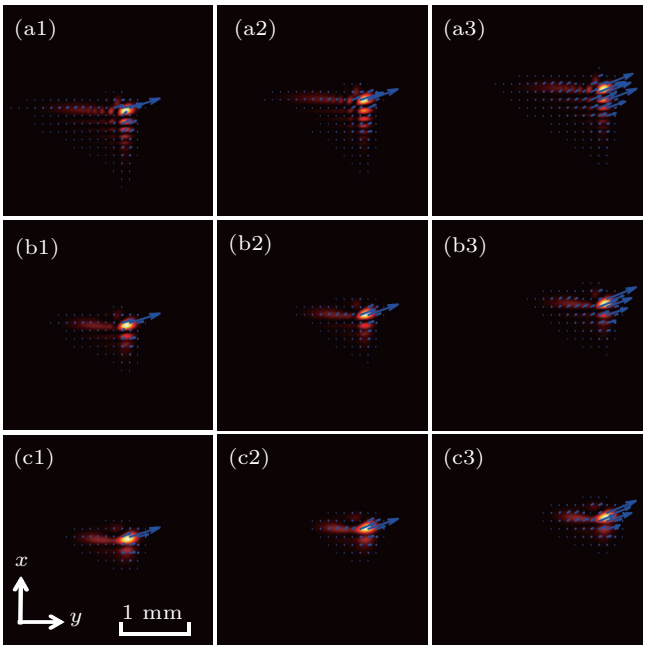


Fig. 4. (color online) The total energy flow (background) and the transverse energy flow (blue arrows) of the LCAiGV beams in uniaxial crystals orthogonal to the optical axis: (a1)–(a3) $\chi_0 = 0.1$ with $n_e = 1.5n_o$, (b1)–(b3) $\chi_0 = 0.2$ with $n_e = 1.5n_o$, (c1)–(c3) $\chi_0 = 0.3$ with $n_e = 1.5n_o$, (a1)–(c1) $\beta_1 = \beta_2 = 1$, (a2)–(c2) $\beta_1 = \beta_2 = 3$, and (a3)–(c3) $\beta_1 = \beta_2 = 5$.

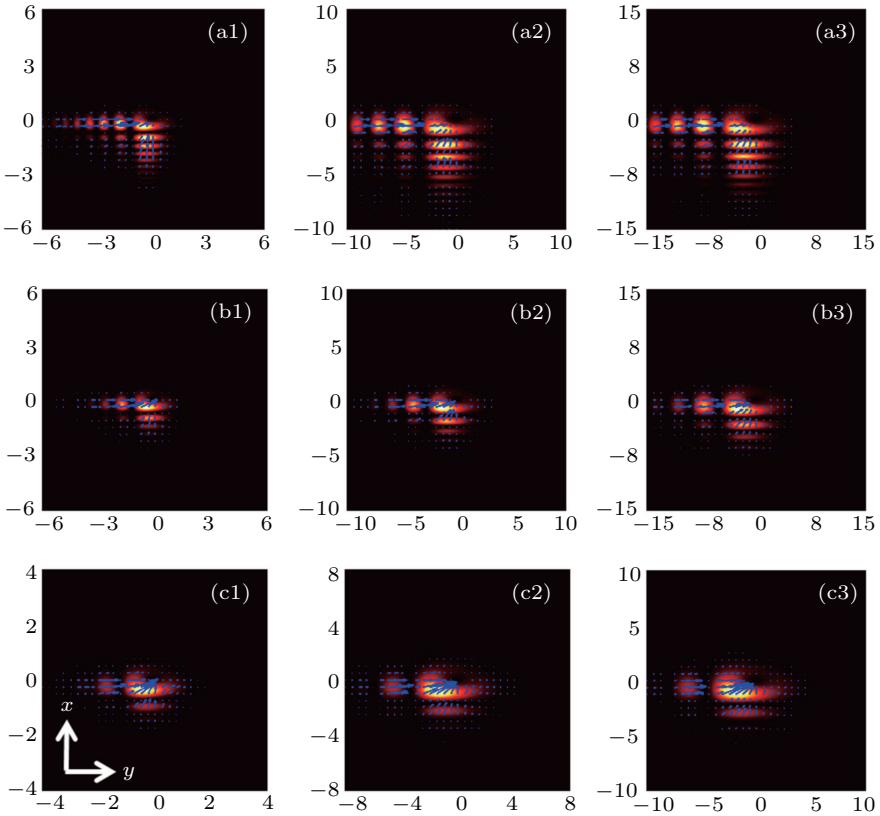


Fig. 5. (color online) The total energy flow (background) and the transverse energy flow (blue arrows) of the QCAiGV beams in uniaxial crystals orthogonal to the optical axis: (a1)–(a3) $\chi_0 = 0.1$ with $n_e = 1.5n_o$, (b1)–(b3) $\chi_0 = 0.2$ with $n_e = 1.5n_o$, (c1)–(c3) $\chi_0 = 0.3$ with $n_e = 1.5n_o$, (a1)–(c1) $\beta_3 = \beta_4 = 1$, (a2)–(c2) $\beta_3 = \beta_4 = 3$, and (a3)–(c3) $\beta_3 = \beta_4 = 5$.

In order to investigate how χ_0 and the linear chirp parameters affect the angular momentum density distribution of the LCAiGV beams, we continue to do a numerical calculation and gain Fig. 6. From Figs. 6(a1)–6(c1), the total momentum density is the same as each other, but the distribution position of the total angular momentum density changes as the linear chirp parameters increase. The angular momentum distributes more along the x axis than that of the y axis in the area of the side lobes. As for all images shown in Fig. 6, the shape of the main lobe seems like an ellipse, and the angular momentum distributes more in the main lobe than that of the side lobes. The arrows of the transverse angular momentum density flow of the LCAiGV beams in the area of the side lobes in the x direction points to the positive x axis, while that in the area of side lobes in the y direction points to the positive y axis direction. In the end, the larger the χ_0 is, the less the number of the side lobes is.

Figure 7 shows the transverse angular momentum distribution of the QCAiGV beams in uniaxial crystals orthogonal to the optical axis. The angular momentum mainly distributes in the side lobes when χ_0 is small enough, as shown in Figs. 7(a1)–7(c1). With the increase of χ_0, the distribution of the angular momentum of the QCAiGV beams gradually turns from the side lobes to the main lobe, and the side lobes are diminishing gradually. More interestingly, the angular momentum density flow of the side lodes of the x direction principally points at the positive y direction, while the angular momentum density flow of the side lodes of the y direction

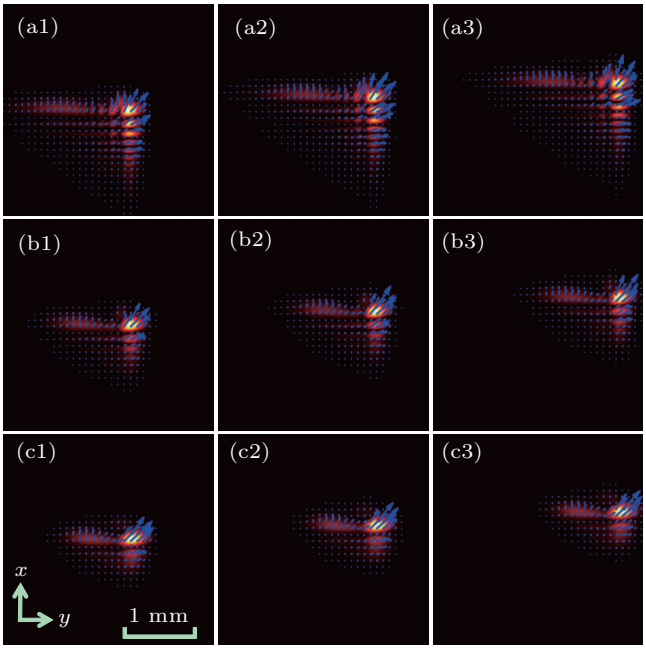


Fig. 6. (color online) The total angular momentum density (background) and the transverse angular momentum density flow (blue arrows) of the LCAiGV beams in uniaxial crystals orthogonal to the optical axis. All the parameters are the same as those in Fig. 4.

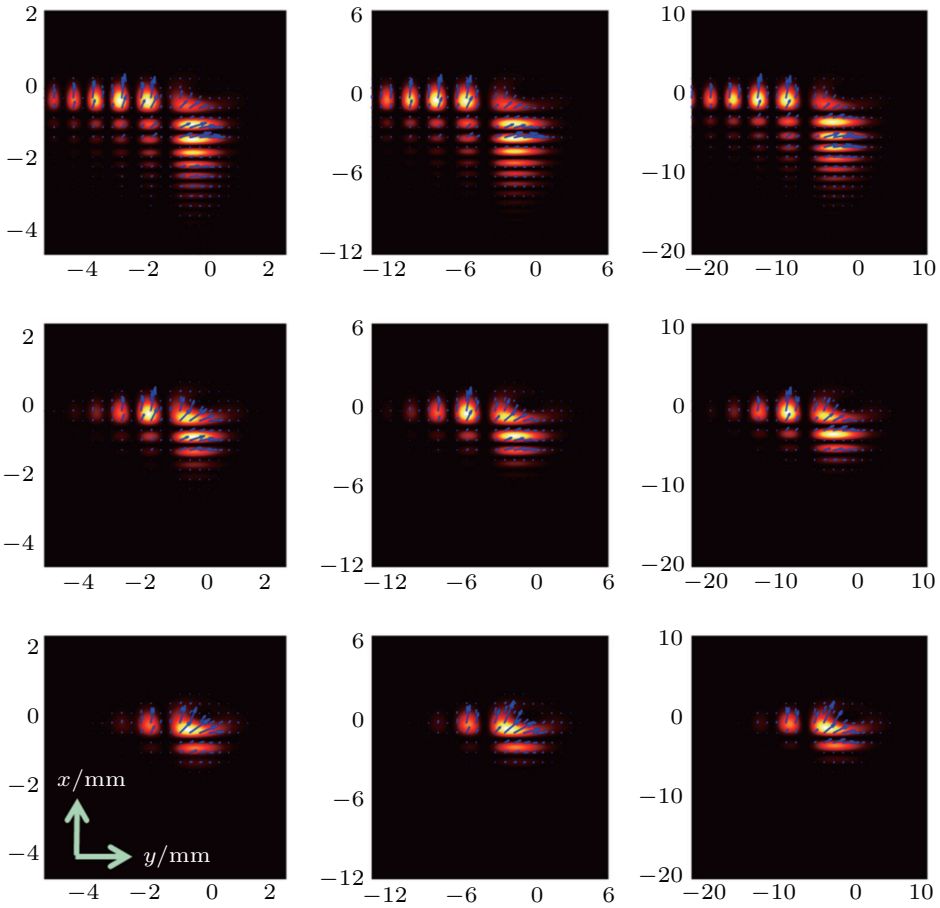


Fig. 7. (color online) The total angular momentum density (background) and the transverse angular momentum density flow (blue arrows) of the QCAiGV beams in uniaxial crystals orthogonal to the optical axis. All the parameters are the same as those in Fig. 5.

principally points at the positive x direction. Meanwhile, the shape of the side lobes of the x direction seems like circular, while that of the y direction seems like an ellipse, indicating that the beam undergoes a compression in the y direction when n_e/n_o is 1.5. The larger the quadratic chirp parameters are, the more dispersed the distribution of the angular momentum of the QCAiGV beams is.

5. Conclusion

In conclusion, we gain analytical expressions of the non-paraxial propagation of the CAiGV beams in uniaxial crystals orthogonal to the optical axis. Some interesting conclusions of the intensity of the CAiGV beams, the LCAiGV beams, and the QCAiGV beams are discovered. The main lobes of the transverse distribution of the intensity, the energy flow density, the angular momentum of the LCAiGV beams are similar to elliptical, while their main lobes of the QCAiGV beams are similar to triangular. Moreover, the transverse distributions of the intensity, the energy flow density, and the angular momentum of the QCAiGV beams are much more dispersed than those of the LCAiGV beams. Besides, the maximum values of the beam intensity are smaller as χ_0 increases. The ranges of the transverse distribution of energy flux density and angular momentum are smaller. We believe that our research results can deepen the understanding of the non-paraxial propagation characteristics of the CAiGV beams in the uniaxial crystals, and can be applied to the modulation of the beams, such as optical particle trapping.

References

[1] Berry M V and Balazs N L 1979 *Am. J. Phys.* **47** 264

[2] Siviloglou G A and Christodoulides D N 2007 *Opt. Lett.* **32** 979

[3] Broky J, Siviloglou G A, Dogariu A and Christodoulides D N 2008 *Opt. Express* **16** 12880

[4] Zhou J X, Liu Y C, Ke Y G, Luo H L and Wen S C 2015 *Opt. Lett.* **40** 3193

[5] Deng D M and Guo Q 2009 *New. J. Phys.* **11** 103029

[6] Deng D, Du S L and Guo Q 2013 *Opt. Commun.* **289** 6

[7] Lin H C and Pu J X 2012 *Chin. Phys. B* **21** 054201

[8] Siviloglou G A, Broky J, Dogariu A and Christodoulides D N 2008 *Opt. Lett.* **33** 207

[9] Yu W H, Zhao R H, Deng F, Huang J Y, Chen C D, Yang X B, Zhao Y P and Deng D M 2016 *Chin. Phys. B* **25** 044201

[10] Deng D M 2011 *Eur. Phys. J. D* **65** 553

[11] Abdollahpour D, Suntsov S, Papazoglou D G and Tzortzakis S 2010 *Phys. Rev. Lett.* **105** 253901

[12] Gu Y L and Gbur G 2010 *Opt. Lett.* **35** 3456

[13] Polynkin P, Koleskik M, Moloney J V, Siviloglou G A and Christodoulides D N 2009 *Science* **324** 229

[14] Huang J Y, Liang Z J, Deng F, Yu W H, Zhao R H, Chen B, Yang X B and Deng D M 2015 *J. Opt. Soc. Am. A* **32** 2104

[15] Chen B, Chen C D, Deng D M and Peng X 2015 *J. Opt. Soc. Am. B* **32** 173

[16] Vasara A, Turunen J and Friberg A T 1989 *J. Opt. Soc. Am. A* **6** 1748

[17] Abramochkin E, Losevsky N and Volostnikov V 1997 *Opt. Commun.* **141** 59

[18] Zhang Y Q, Beli M R, Zhang L, Zhong W P, Zhu D Y, Wang R M and Zhang Y P 2015 *Opt. Express* **23** 10467

[19] Ciattoni A, Cincotti G and Palma C 2002 *J. Opt. Soc. Am. A* **19** 1422

[20] Deng F and Deng D M 2016 *Opt. Commun.* **380** 280

[21] Zhang J B, Zhou K Z, Liang J H, Lai Z Y, Yang X B and Deng D M 2018 *Opt. Express* **26** 1290

[22] Ciattoni A and Palma C 2003 *J. Opt. Soc. Am. A* **20** 2163

[23] Sztul H I and Alfano R R 2008 *Opt. Express* **16** 9411